Hindawi
International Journal of Antennas and Propagation
Volume 2022, Article ID 4663488, 12 pages
https://doi.org/10.1155/2022/4663488

Research Article

On the Design and Development of Planar Monopole Antenna for Bone Crack/Void Detection

Ananda Venkatesan Boologam, Kalimuthu Krishnan, Sandeep Kumar Palaniswamy, Sachin Kumar, Shreya Bhowmik, Nivesh Sharma, Deepesh Vaish, and Sourish Chatterjee

Department of Electronics and Communication Engineering, SRM Institute of Science and Technology, Kattankulathur, 603203, India

Correspondence should be addressed to Kalimuthu Krishnan; kalimutk@srmist.edu.in and Sandeep Kumar Palaniswamy; vrpchs@gmail.com

Received 23 July 2021; Revised 21 January 2022; Accepted 4 April 2022; Published 5 May 2022

Academic Editor: Hervé Aubert

In this study, the design of a compact narrowband monopole antenna for bone crack detection is presented. The proposed antenna consists of a modified hexagon-shaped radiator with six triangular slits integrated on its bottom periphery, a rectangular-shaped ground plane, and a microstrip feed line of 50 Ω. The antenna is fabricated on the FR-4 substrate with a thickness of 1.6 mm, an overall size of 32 mm × 30 mm, and electrical dimensions of $0.13\lambda_0 \times 0.122\lambda_0$, where λ_0 is the free space wavelength at 2.45 GHz. The resonant frequency of the designed antenna is 2.45 GHz. The antenna offers a gain of 1.68 dB and an efficiency of 85.3%. The presence of a crack in the bone is detected by observing the shift in the peak resonating frequency of the antenna. This method can detect bone fractures in a noninvasive manner. The human arm model is constructed, and the effect of bone cracks of different lengths on the resonating frequency is investigated. The pig bone and tissues are used to validate the simulated results. The simulated results are in agreement with the measured outcomes. Also, the specific absorption rate (SAR) of the antenna is calculated and found to be less than 0.57 W/kg. The designed monopole antenna has several advantages, including a small footprint, straightforward design, low cost, and easy integration with other devices. The proposed method is suitable for primary-level bone crack diagnosis.

1. Introduction

The importance of bones in the human body is well understood. They perform important functions such as mineral storage and providing mechanical strength to soft tissues and organs. A bone fracture can occur for a variety of reasons. Osteoporosis, caused by a lack of vitamin D, causes bone brittleness, which can lead to bone cracks. An accident also can cause fractures or defects in human bones. The tibia, also known as the shinbone, is the longest bone in the human body and is located in the lower part of the leg. There is a higher possibility for the occurrence of a tibia fracture. Tibia fractures are common in children, athletes, and the elderly, and they are difficult to detect at the outset [1]. The uncontrolled movement of a fractured part may aggravate the injury. Therefore, detecting bone fractures at an early stage is expected as the restricted activity of the affected region can aid in the rapid healing of the fractured part. Techniques such as X-ray, ultrasound, computed tomography, and magnetic resonance imaging can be used to detect fracture. X-ray is the most commonly used method for detecting bone cracks. However, frequent exposure of the human body to X-rays may increase the risk of cancer. An ultrasound uses nonionized radiations to detect fractures, but the presence of speckles reduces image resolution, which affects diagnosis accuracy, and ultrasonic waves are highly attenuated by multiple layers of the human body. Computer tomography uses ionized radiation for diagnosis, which has the potential to cause cancer in pediatric patients. The magnetic resonance technique requires a complicated system, skilled technicians, and a high operating cost. However, due to high radiation levels, these

techniques are not suitable for children and pregnant women. Therefore, a more efficient, noninvasive, safe, and nonionized radiation method is required for detecting bone fractures [2].

Microwaves, unlike ultrasonic waves, can easily penetrate and are not attenuated by multiple layers of the human body having different dielectric constant values. This feature of microwaves attracts planar antennas for medical diagnosis. The International Telecommunication Union (ITU) has recommended that the frequency bands 401–406 MHz, 433.1–434.8 MHz, 608–614 MHz, 868–868.6 MHz, 902.8–928 MHz, 1.395–1.4 GHz, 1.427–1.432 GHz, and 2.45–2.5 GHz, popularly known as industrial, scientific, and medical (ISM) bands, can be used for medical implant communication services [3, 4]. Since the human body is made up of layers with different dielectric constants, an antenna resonating at lower frequencies will have a greater depth of penetration. However, antennas operating at lower frequencies may have larger dimensions [5]. Composite left/right-handed materials have been used in the design of sensing antennas due to their unique properties such as uniform group velocity, zero attenuation, and constant phase [6–8]. Several techniques, such as high-permittivity substrates and reactive elements, have also been used to design compact diagnostic/sensing antennas. In [9], a metamaterial-based antenna array was used for detecting tumors in breast tissues. In this method, the antennas were placed around the breast model, with one antenna acting as a transmitter at a time and the other antennas acting as receivers. The receiver antennas adjacent to the transmitter antennas receive the signal reflected from the tissue surface, while the opposite-side antennas collect the signal that traveled through the breast tissue. In this manner, the magnitude and phase information of the scattered signal were captured, and this information was then used for the dielectric characterization of the breast tissues.

Once a bone crack has occurred, it is necessary to monitor the affected area on a regular basis to ensure quick restoration and healing. Fracture healing can be monitored by passing current through the implanted pins and recording the variation in impedance to determine the level of recovery. The impedance decreases when the bone fracture is restored after three to four weeks [10]. However, the disadvantage of this method is that the variation in impedance level is small, and making differentiation is a difficult task. In another technique [11], some of the electromagnetic properties of the bone, such as dielectric constant, inductance, and conductance, were used to monitor fracture healing. In this method, two monopoles were placed across the fractured part, and the amount of power received was measured. When the bone crack was large in size, the power received was initially low, but it gradually increases as the crack healed. Microwave imaging allows the noninvasive diagnosis of biological tissues while also being low in cost and risk of manipulation. The microwave tomographic system identifies variations in dielectric constants between tissue and bones, and the rapid localization of the dielectric frontier allows image construction of the bone structure [12]. The authors of [13] designed a microwave ring resonator for bone fracture detection, wherein the affected region was scanned and variations in transmission characteristics were used to characterize the fracture. When the antenna/resonator is placed closer to the human body, some of its performance characteristics, such as resonant frequency, gain, and efficiency, slightly deviate from their actual values [14–16]. However, the absorption of electromagnetic radiation by the human body is a major concern, and if it exceeds certain limits, it may cause health issues [17]. In biomedical applications, an antenna can be used as an implantable or on-body device to detect disease or abnormalities in organs. An implantable antenna should be biocompatible and small in size [18]. Several decades ago, implanted devices were powered, controlled, and monitored by external stations linked by wired connections, which could result in unavoidable surgical complications. Modern antenna technology significantly reduces the issue of surgical risk to human life [19]. A monopole antenna is an excellent candidate for detecting disease/abnormalities in the human body due to its straightforward design, simple fabrication on the dielectric substrate, small size, low cost, easy integration with other devices, and improved performance in multipath environments [20–23]. Also, the various performance metrics of the monopole antenna, such as impedance bandwidth, gain, and efficiency, can be easily controlled by altering the ground shape and adjusting the gap between the radiator and ground plane [24–26].

This study presents the design of a narrowband monopole antenna for bone fracture detection. The antenna prototype is tested on the pig bone, and the effect of different length bone cracks on the resonating frequency is investigated. This manuscript is divided into five sections. Section 1 discusses various causes of bone cracks, different methods of fracture detection, and their benefits and drawbacks. Section 2 describes the antenna design procedure and parametric specifications. Section 3 describes the structure of the human arm model, specific absorption rate (SAR), and antenna characteristics in different environments. Section 4 discusses the bone fracture detection process and the results obtained, and Section 5 provides the conclusion.

2. Antenna Design

The proposed monopole antenna is shown in Figure 1. The radiator and ground plane are printed on the front and back sides of the FR-4 material with a thickness of 1.6 mm, dielectric constant of 4.4, and loss tangent of 0.02. The antenna consists of a modified hexagon-shaped radiator with six triangular slits integrated on its bottom periphery, a rectangular-shaped ground plane, and a microstrip feed line of the width of 3.1 mm to match the 50 Ω impedance. The final structure of the antenna is obtained after four stages of evolution. The fabricated antenna prototype is shown in Figure 2. The physical size of the antenna is 32 mm × 30 mm, and its electrical dimensions are $0.13\lambda_0 \times 0.122\lambda_0$, where λ_0 is the free space wavelength at 2.45 GHz. The 3D EM simulator CST Microwave Studio® is used for simulating the antenna design.

The evolution of the proposed antenna is shown in Figure 3. A rectangle and a hexagon are combined to form a radiator in the first stage, as shown in Figure 3(a). The antenna is excited by a microstrip line, and a rectangular-

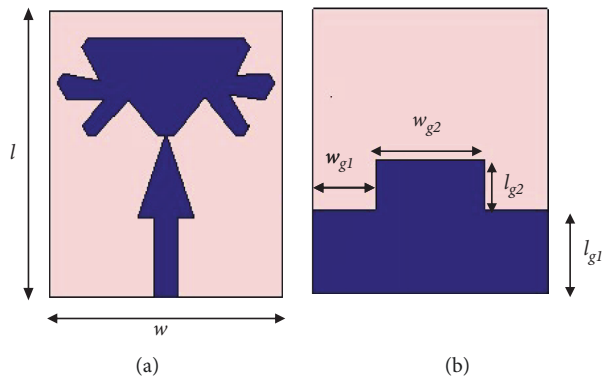

Figure 1: Proposed monopole antenna. (a) Front plane. (b) Back plane ($l = 32$ mm, $w = 30$ mm, $l_{g1} = 9.4$ mm, $l_{g2} = 5.6$ mm, $w_{g1} = 8$ mm, and $w_{g2} = 14$ mm).

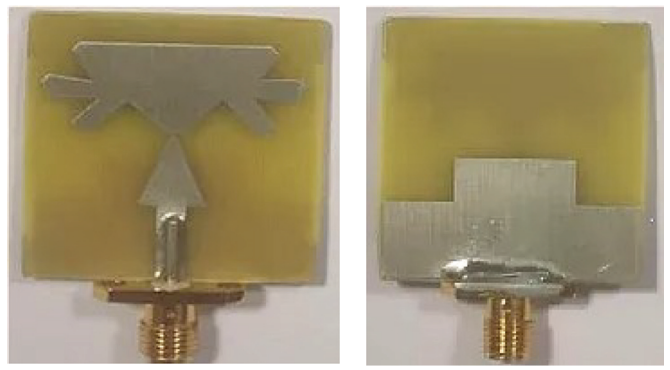

Figure 2: Fabricated antenna prototype. (a) Front view. (b) Rear view.

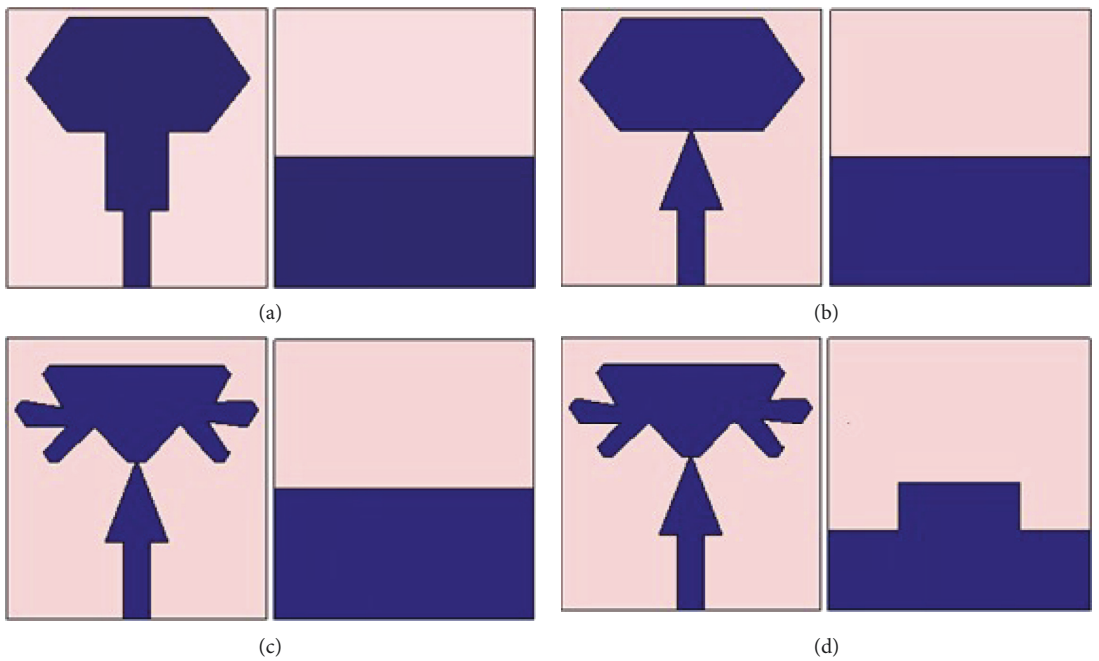

Figure 3: Evolution stages of the antenna. (a) Stage 1. (b) Stage 2. (c) Stage 3. (d) Stage 4.

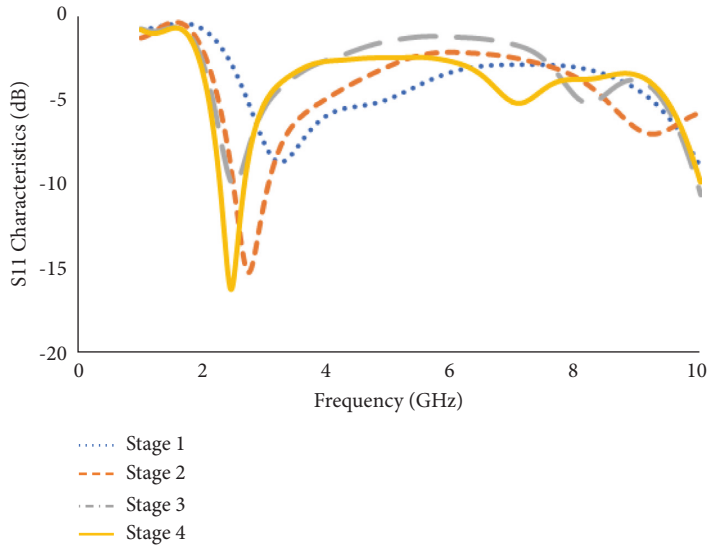

Figure 4: Reflection coefficient characteristics of the antenna stages.

shaped partial ground plane is designed on the backside of the substrate. In the first stage of evolution, the antenna shows a resonance at 3.24 GHz, but the impedance matching is poor at this frequency. The rectangular patch is then tapered in order to concentrate the charge carriers in a specific portion of the radiator, resulting in a resonant frequency shift to 2.74 GHz, as shown in Figure 3(b). In the third stage, six triangular slits are introduced in the bottom periphery of the radiator (shown in Figure 3(c)) to increase the length of the current path. In the next stage, rectangular slits are cut into the ground plane, reducing capacitive reactance, and allowing the antenna to resonate at 2.458 GHz with a reflection coefficient of −16.28 dB, as shown in Figure 3(d). Figure 4 depicts the reflection coefficient characteristics at various stages of evolution.

To understand the theoretical aspects of the antenna, the equivalent circuit model and surface current distribution are studied. Figure 5(a) depicts the electrical equivalent circuit of the designed antenna, and Figure 5(b) shows the real and imaginary impedance characteristics of the antenna. Both the real and imaginary curves move from high to low at 2.45 GHz resonant frequency resulting in a parallel combination of R, L, and C components in the circuit model.

The surface current distribution is depicted in Figure 6. It shows that the current density of 2.45 GHz is highly concentrated in the triangular slit region.

The E-plane and H-plane radiation patterns of the designed antenna are shown in Figures 7(a) and 7(b), respectively. The figure clearly shows that the antenna produces an omnidirectional radiation pattern at 2.45 GHz. The measured gain and radiation efficiency of the antenna are shown in Figure 8. The gain of the antenna is 1.68 dB, and its efficiency is 85.3%.

3. System Description

3.1. Human Arm Model. The human arm consists of four layers as shown in Figure 9. The bone is the innermost layer, and the skin is the outermost layer. Muscle and fat are found between these two layers. Each layer has different relative permittivity, conductivity, and loss tangent values, which are listed in Table 1 [27].

3.2. SAR. Since the human body is made up of many layers with different conductive and dielectric properties, and when the antenna is operated closer to the human body, some of the radiated power is absorbed by the body, which may result in higher SAR [28–30].

The SAR is an important parameter that quantifies the amount of electromagnetic energy absorbed by body tissues. The standard unit for measuring SAR is W/kg.

$$\text{SAR} = \frac{\sigma |E|^2}{\rho} \text{ W/kg}, \tag{1}$$

where E is the root mean square of the electric field (V/m), σ is the conductivity (S/m), and ρ is the mass density of the tissue (kg/m^3).

According to the FCC guidelines, the SAR should be less than 1.6 W/Kg, and the simulated SAR value for the designed antenna is <0.812 W/Kg. The SAR of the proposed monopole antenna is depicted in Figure 10.

In order to measure the SAR, microwave signals with 1 mW power are applied to the antenna, and the thermogram readings are taken before and after (20 minutes) excitation.

$$\text{SAR} = \frac{\Delta T}{\Delta t} C_t \text{ W/kg}, \tag{2}$$

where ΔT is the rise in the temperature (°C), Δt is the time duration for which microwave signals are applied (second), and C_t is the heat capacity (J/kg/°C) of different parts, such as skin, fat, muscle, and bone.

The temperature rose from 34.1°C to 34.3°C after 1,200 seconds of excitation, and the increase in temperature by

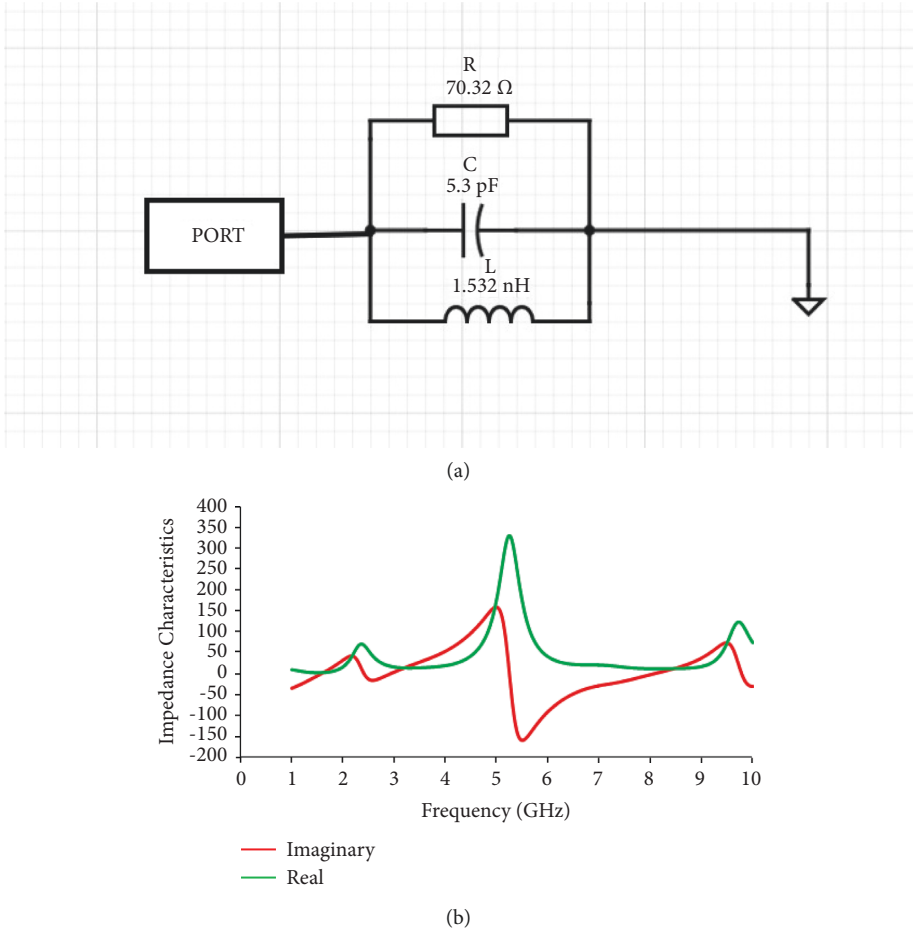

Figure 5: Equivalent circuit study. (a) Circuit model. (b) Real and imaginary characteristics.

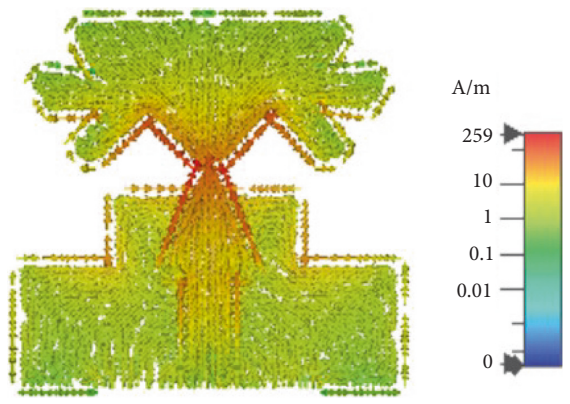

Figure 6: Surface current distribution of the antenna at 2.45 GHz.

0.2°C remained the same for a long duration of time. Then, the SAR of the antenna is calculated, using expression (2), as 0.57 W/kg.

3.3. Antenna Characteristics along with the Arm Model. When the antenna is simulated in free space, the peak resonance is noticed at 2.458 GHz. If the same antenna is placed on the arm model that does not have a crack, the resonant frequency shifts to the lower side at 2.124 GHz [31], as shown in Figure 11.

4. Bone Fracture Detection

The antenna is placed on the arm model to detect bone cracks. Cracks of varying lengths are induced in the bone model, and the changes in the reflection coefficient characteristics of the antenna are noted. The length of the bone crack is determined by the amount of shift of the resonating band.

The dielectric properties, such as permittivity (ε_r) and permeability (μ_r), play an important role in the material characterization. The dielectric properties of a material can be influenced by factors such as density, structure deformation, water content, and porosity. The speed of propagation of an electromagnetic wave is determined by the permittivity of the medium through which it travels and interacts with the material in three ways: absorption, reflection, and transmission. The amount of reflection depends on the permittivity of the material and the frequency of the propagating microwave signal.

In the presented work, the electromagnetic radiations are used to characterize the dielectric properties of the bone structure without causing any destruction. The obtained

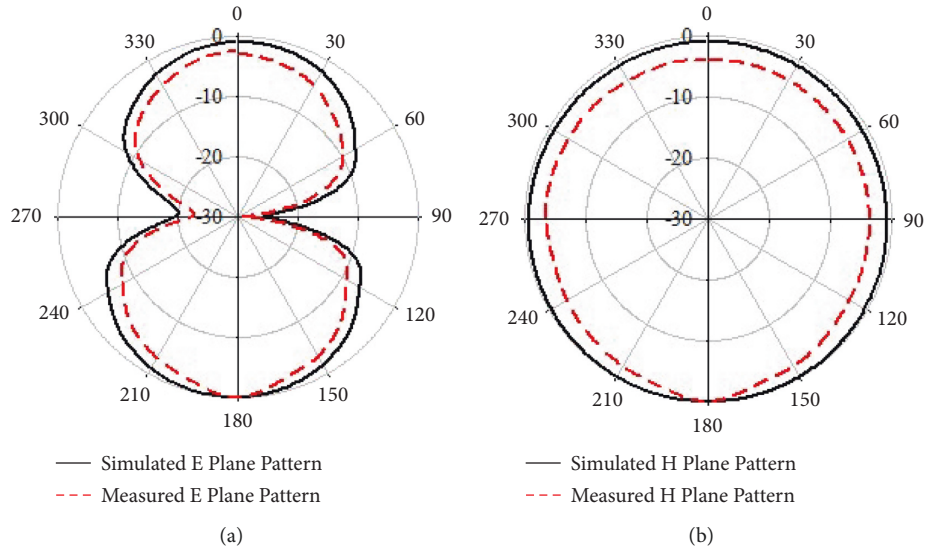

Figure 7: Radiation patterns at 2.45 GHz. (a) E-plane. (b) H-plane.

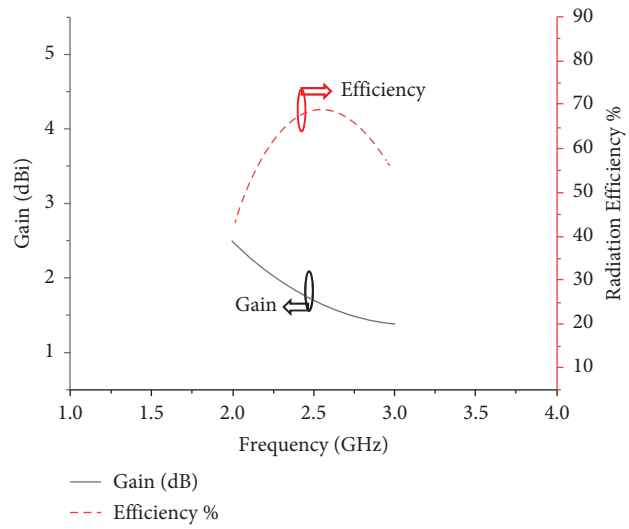

Figure 8: Measured gain and efficiency of the proposed antenna.

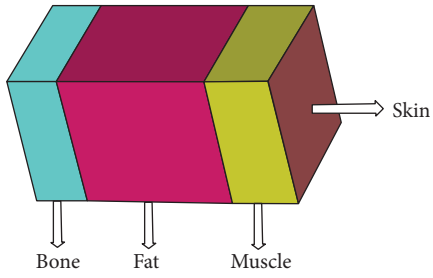

Figure 9: Human arm model.

reflection coefficients are analyzed to detect changes in the bone profile. There is a difference in the peak value of the reflection coefficients between the bone with and without a crack. The amount of frequency deviation is proportional to the crack's dimension. This is due to the fact that if a crack exists, the permittivity of the bone changes, affecting the reflection coefficient characteristics.

$$\Gamma = \frac{Z_L - Z_0}{Z_L + Z_0} = \frac{\sqrt{(\mu_r/\varepsilon_r)} - 1}{\sqrt{(\mu_r/\varepsilon_r)} + 1}, \tag{3}$$

where

$$Z_L = \exp\left(j\omega\sqrt{(\mu_r\varepsilon_r)}\, d\right). \tag{4}$$

When the antenna is placed over the arm model without a bone crack, the reflections of the radiations are only due to bone having relative permittivity of 12.66. If a crack is present in the bone (i.e., air is the medium in the crack), the S_{11} characteristics are determined by the effective dielectric constant of the bone and the air gap.

Table 1: Characteristics of various layers of human arm.

Layer	Thickness (mm)	Relative permittivity (mm)	Loss tangent	Density (kg/m^3)
Skin	0.4	41.4	0.418	1100
Fat	30	5.46	0.186	1100
Muscle	69.6	55	0.342	1040
Bone	13	18.49	0.214	1008

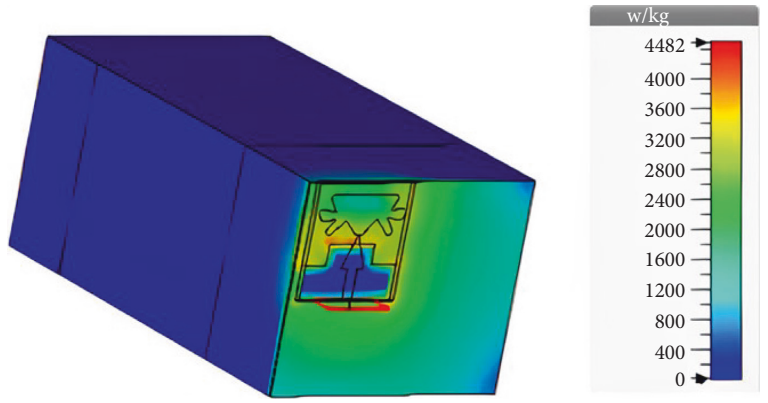

Figure 10: SAR analysis.

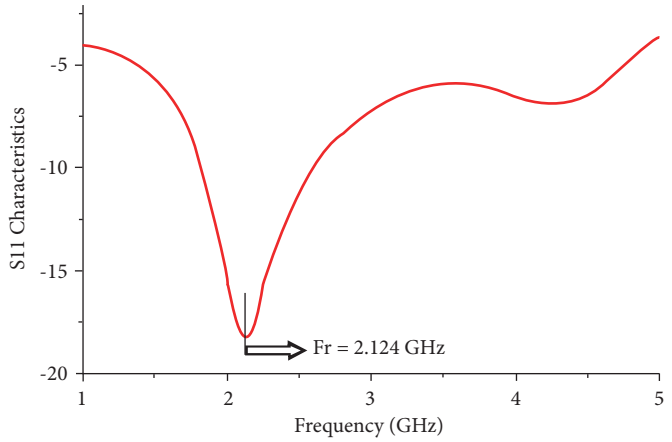

Figure 11: Reflection coefficients when the antenna is placed closer to the human arm.

For a crack length of 2 mm, the antenna shows a resonant peak at 2.132 GHz. The resonant frequency moves to the higher side as the bone crack length increases, and for a crack length of 10 mm, the resonance shifts to 2.16 GHz, as shown in Figure 12. This is due to the fact that when a crack is present, the radiation from the antenna is reflected by two mediums with different dielectric constants (12.66 and 1). The resonant frequencies for different fracture lengths are presented in Table 2.

The antenna is fabricated, and its reflection coefficients are measured using VNA. When used in free space, the antenna shows the peak resonance at 2.45 GHz, and when positioned closer to the human arm, as shown in Figures 13 and 14, the resonance is achieved at 2.122 GHz.

Also, a portion of pig bone and tissue was used to validate the simulated results. Fractures of varying lengths were induced, the fabricated antenna was placed over the pig bone (Figure 15), and the corresponding changes in the reflection coefficients are shown in Figure 16. The measurements show that the experimental values are consistent with the simulated values for different fracture lengths.

Pig bone and tissues were chosen for the bone crack detection process due to their similarities to human bone and tissues. The antenna ground plane is placed on the skin, and the resonance frequency is measured using the VNA. Without a bone crack, the antenna produces resonance at 2.122 GHz, which is nearly identical to the simulated resonance at 2.124 GHz. Then, in the pig bone, fractures of various lengths such as 10 mm, 20 mm, and 30 mm were induced, and the change in the reflection coefficient characteristics was examined, as shown in Figure 17. The difference between the obtained frequency (f_n) and no crack frequency (f_c) is calculated, as shown in Table 3, and plotted on the x-axis (frequency difference (d_f), GHz) and crack/fracture length (mm) on the y-axis, as shown in Figure 18. The obtained

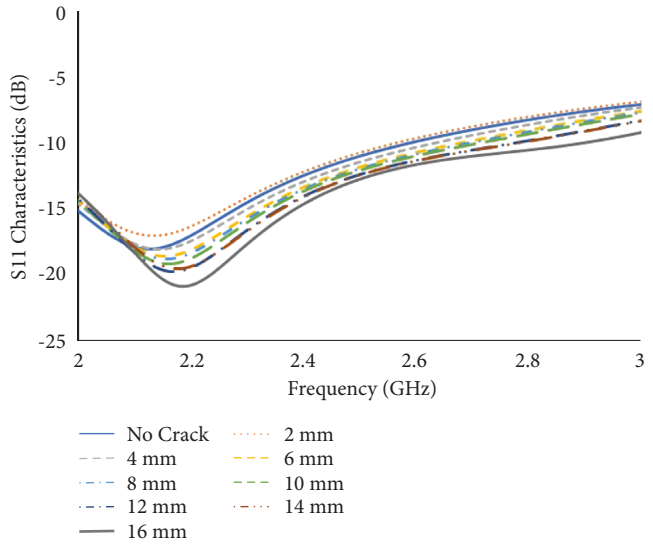

Figure 12: Resonant frequencies for different fracture lengths.

Table 2: Resonant frequencies for different fracture lengths.

Void size	Freq. (GHz)	Shift (in MHz)	Void size (in mm)	Freq. (GHz)	Shift (in MHz)
0	2.124	—	—	—	—
2	2.132	8	10	2.16	36
4	2.144	20	12	2.168	44
6	2.152	28	14	2.176	52
8	2.156	32	16	2.184	60

Figure 13: Measurement setup using a VNA.

frequency deviation is 0.03 GHz or 30 MHz, which is good enough to differentiate crack lengths. Also, a linear relationship is established between fracture length (mm) and frequency deviation (GHz), as shown in equation (5).

$$\text{Fracture length} = 278.2 \times \left(d_f\right) - 0.64, \tag{5}$$

where d_f is the difference in frequency.

The presented work is compared to recently published work in Table 4, and the highlights and advantages of the proposed antenna system are as follows:

(i) The conventional fracture diagnosis methods, such as X-ray, ultrasound, computed tomography, and magnetic resonance imaging, use ionized radiations, which may pose health risks to humans. In this work, an

Figure 14: On-body testing of the antenna.

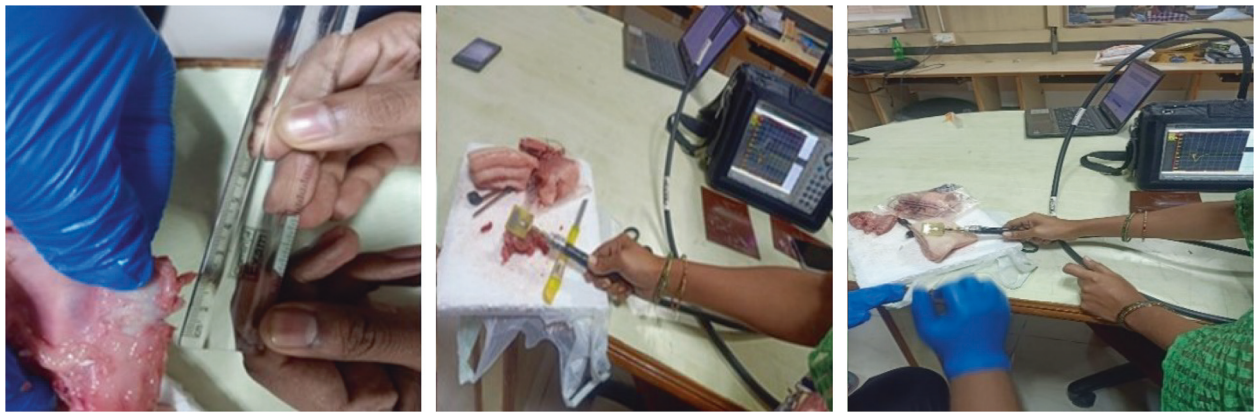

Figure 15: Measurement of S11 parameters on pig bone.

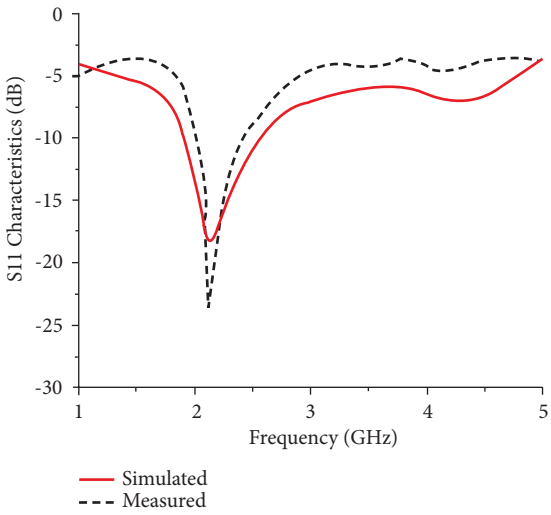

Figure 16: Reflection coefficient of the antenna on pig bone.

efficient, noninvasive, safe, and nonionized radiation method is proposed for detecting bone fractures.

(ii) A planar monopole antenna operating at the ISM band is designed for bone crack detection. Microwaves, unlike ultrasonic waves, can easily penetrate and are not attenuated by the multiple layers of the human body with different dielectric constant values. This method noninvasively detects bone fractures and does not require any additional circuitry to process the data. The antenna prototype is tested on the pig bone, and the effect of different length bone cracks on the resonating frequency is investigated. A linear relationship is found between crack length (mm) and frequency deviation (GHz).

(iii) When designing the antenna, care has been taken to keep the SAR below 1.6 W/kg, as the antenna is operating in close proximity to the human body. Microwaves may be absorbed by human tissues, and microwave absorption above a certain threshold may pose health risks.

(iv) A compact planar monopole antenna, with a size of 32 mm × 30 mm, is designed to radiate at 2.45 GHz for bone crack detection.

(v) The proposed bone crack detection method does not require any additional processing units.

(vi) Fresh pig bone (rather than the human bone) was used to validate the simulated results, whereas in other works, the authors did not validate the simulated results or use artificial bone models or old human bones for measurements.

(vii) Since the antenna is operating in close proximity to the human body, microwaves may be absorbed by human tissues, and microwave absorption above a certain threshold may pose health risks. When designing the antenna, care has been taken to keep the SAR below 0.57 W/kg.

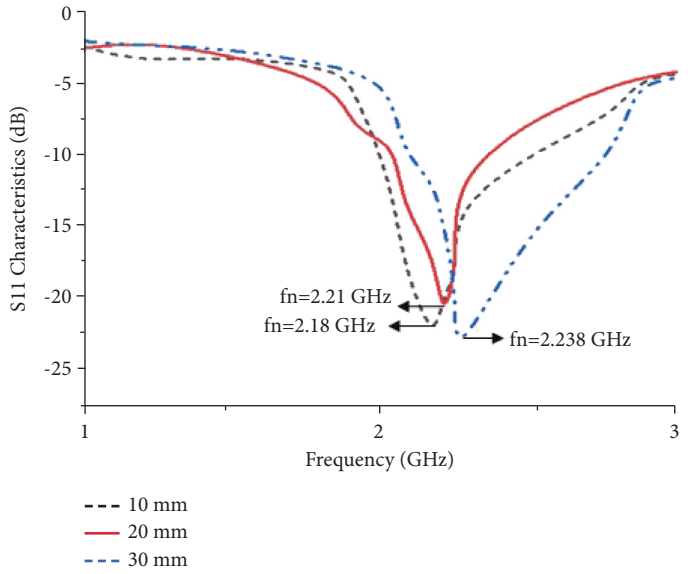

Figure 17: Measured reflection coefficients for different fracture lengths.

Table 3: Details of the frequency difference/shift.

Crack length (mm)	Peak resonance (GHz) (f_n, where $n = 1, 2, 3, 4$)	Frequency difference (GHz) ($d_f = f_n - f_c$)
No crack	$2.122 = f_c$	—
10	2.18	0.058
20	2.21	0.088
30	2.238	0.166

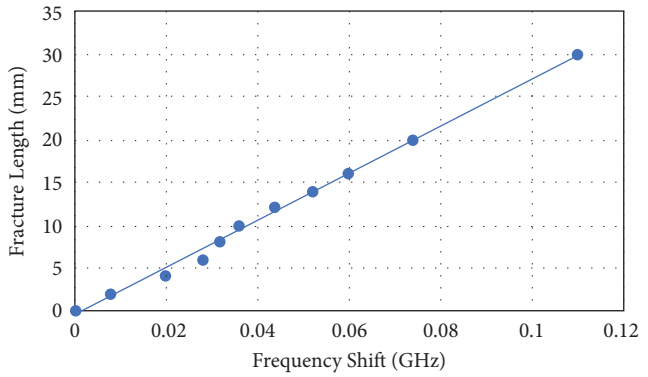

Figure 18: Variation of frequency shift with the fracture length.

Table 4: Comparison of the reported antenna designs with the proposed antenna.

Parameters	[8]	[9]	[10]	[11]	Proposed
Antenna type	Implantable monopole	Antipodal vivaldi	Microwave ring resonator	Microstrip patch	Planar monopole
Operating frequency (GHz)	1 to 4	0.5 to 4	2.45	2.45	2.45
Dimensions (mm × mm), ($\lambda_0 \times \lambda_0$)	60×55, 0.2×0.18	100×50, 0.167×0.083	80×114, 0.25×0.45	48.7×55.9, 0.2×0.22	32×30, 0.128×0.12
Sensitivity	Moderate	Moderate	High	Low	Moderate
SAR (W/kg)	—	—	<1.6	—	<0.812
Experimental validation done	Yes	Yes	Yes	No	Yes
Requirement of an additional processing unit	No	Yes	Yes	No	No

The proposed monopole antenna can be an excellent candidate for detecting bone cracks due to its straightforward fabrication on the dielectric substrate, small size, low cost, ease of integration with other devices, improved performance in multipath environments, and ease of operation as special skills are not required to use such device.

5. Conclusions

A planar monopole antenna is designed and developed for bone crack detection applications. The proposed antenna produces an omnidirectional radiation pattern with a gain of 1.68 dB and an efficiency of 85.3%. The EM simulator CST Microwave Studio® is used to simulate the human arm model, with fractures of varying lengths introduced. The designed antenna is scanned over the arm model, and the changes in the reflection coefficient characteristics are examined. The pig bone is used for the measurement, with cracks of varying lengths introduced and variations in the reflection coefficients investigated. The measured values agree well with the simulated results. It is observed that the resonant frequency of the antenna shifts to the higher side as the crack length increases. As the crack length increases from 10 mm to 30 mm, the corresponding resonance frequency shifts from 2.18 GHz to 2.38 GHz. Therefore, the frequency deviation is used to quantify the length of the fracture. Also, a linear expression is obtained for measuring the crack length as a function of frequency deviation. The SAR value of the proposed antenna is less than 0.57 kg/W. The presented method could be a low-cost RF solution for bone fracture detection.

Data Availability

Data are available on request.

Conflicts of Interest

The authors declare that there are no conflicts of interest regarding the publication of this paper.

References

[1] J. Kenwright, J. Richardson, J. Cunningham et al., "Axial movement and tibial fractures. A controlled randomised trial of treatment," *Journal of Bone & Joint Surgery, British Volume*, vol. 73-B, no. 4, pp. 654–659, 1991.

[2] Y. Bishitz, N. Ozana, Y. Beiderman et al., "Noncontact optical sensor for bone fracture diagnostics," *Biomedical Optics Express*, vol. 6, no. 3, pp. 651–657, 2015.

[3] A. W. Damaj, H. M. El Misilmani, and S. A. Chahine, "Implantable antennas for biomedical application, an overview on alternative antenna design methods and challenges," in *Proceedings of the International Conference on High Performance Computing & Simulation (HPCS)*, pp. 31–37, Orleans, France, July 2018.

[4] E. Avila-Navarro1 and C. Reig, "Directive microstrip antennas for specific Below–2.45 GHz applications," *International Journal of Antennas and Propagation*, vol. 2012, Article ID 612170, 6 pages, 2012.

[5] S. Symeonidis, W. G. Whittow, C. Panagamuwa, and M. Zecca, "An implanted antenna system for the monitoring of the healing of bone fractures," in *Proceedings of the Loughborough Antennas & Propagation Conference (LAPC)*, pp. 1–4, Loughborough, UK, November 2015.

[6] M. Alibakhshikenari, B. S. Virdee, A. Ali, and E. Limiti, "Extended aperture miniature antenna based on CRLH metamaterials for wireless communication systems operating over UHF to C-band," *Radio Science*, vol. 53, no. 2, pp. 154–165, 2018.

[7] M. A. Kenari, "Printed planar patch antennas based on metamaterial," *International Journal of Electronics Letters*, vol. 2, no. 1, pp. 37–42, 2014.

[8] M. Alibakhshikenari, B. S. Virdee, A. Ali, and E. Limiti, "A novel monofilar-Archimedean metamaterial inspired leaky-wave antenna for scanning application for passive radar systems," *Microwave and Optical Technology Letters*, vol. 60, no. 8, pp. 2055–2060, 2018.

[9] M. Alibakhshikenari, B. S. Virdee, P. Shukla et al., "Metamaterial-Inspired antenna array for application in microwave breast imaging systems for tumor detection," *IEEE Access*, vol. 8, Article ID 174667, 2020.

[10] M. C. Lin, D. Hu, M. Marmor, S. T. Herfat, C. S. Bahney, and M. M. Maharbiz, "Smart bone plates can monitor fracture healing," *Scientific Reports*, vol. 9, no. 1, pp. 2122–2215, 2019.

[11] S. Symeonidis, W. G. Whittow, M. Zecca, and C. Panagamuwa, "Bone fracture monitoring using implanted antennas in the radius, tibia and phalange heterogeneous bone phantoms," *Biomedical Physics & Engineering Express*, vol. 4, no. 4, Article ID 45006, 2018.

[12] G. Ruvio, A. Cuccaro, R. Solimene, A. Brancaccio, B. Basile, and M. J. Ammann, "Microwave bone imaging: a preliminary scanning system for proof-of-concept," *Healthcare Technology Letters*, vol. 3, no. 3, pp. 218–221, 2016.

[13] V. S. Ramalingam, M. Kanagasabai, and E. F. Sundarsingh, "A compact microwave device for fracture diagnosis of the human tibia," *IEEE Transactions on Components, Packaging, and Manufacturing Technology*, vol. 9, no. 4, pp. 661–668, 2019.

[14] G. M. Jagan, N. Arun Palanikumar, A. C. Varun Miranda, and S. Esther Florence, "Development of A Planar sensor for monitoring orthopaedic health," *International Journal of Advance Computational Engineering and Networking (IJACEN)*, vol. 4, no. 5, pp. 24–28, 2016.

[15] V. S. Ramalingam, M. Kanagasabai, and E. F. Sundarsingh, "Detection of voids in fiber reinforced plastics using magnetoinductive coupled microstrip sensor," *IEEE Sensors Journal*, vol. 15, no. 8, pp. 4182-4183, 2015.

[16] M. K. Sharma, M. kumar, J. P. Saini, D. Kanaujia, S. P. Singh, and A. L. Ekuakille, "Experimental investigation of the breast phantom for tumor detection using ultra-wide band-MIMO antenna sensor (UMAS) probe," *IEEE Sensors Journal*, vol. 20, no. 12, pp. 6745–6752, 2020.

[17] S. Kumari and V. R. Gupta, "Measurement of specific absorption rate of monopole patch antenna on human arm," *International Journal of Microwave and Optical Technology*, vol. 10, no. 3, 2015.

[18] S. M. Abbas, Y. Ranga, and K. P. Esselle, "Reconfigurable antenna options for 2.45/5 GHz wireless body area networks in healthcare applications," in *Proceedings of the 2015 37th Annual International Conference of the IEEE Engineering in Medicine and Biology Society (EMBC)*, pp. 5465–5468, Milan, Italy, August 2015.

[19] A. Gupta, A. Kansal, and P. Chawla, "A survey and classification on applications of antenna in health care domain: data

transmission, diagnosis and treatment," *Sādhanā*, vol. 46, no. 2, pp. 68–17, 2021.

[20] M. M. Soliman, M. E. H. Chowdhury, A. Khandakar et al., "Review on medical implantable Antenna technology and imminent research challenges," *Sensors*, vol. 21, no. 9, pp. 3163–3228, 2021.

[21] S. Ashok Kumar and T. Shanmuganantham, "Design of clover slot antenna for biomedical applications," *Alexandria Engineering Journal*, vol. 56, no. 3, pp. 313–317, 2017.

[22] M. Ahmed, C. H. See, I. M. Danjuma et al., "An active microwave sensor for near field imaging," *IEEE Sensors Journal*, vol. 17, no. 9, pp. 2749–2757, 2017.

[23] M. Alibakhshi-Kenari, M. Naser-Moghadasi, and R. Sadeghzadeh, "The resonating MTM-based miniaturized antennas for wide-band RF-microwave systems," *Microwave and Optical Technology Letters*, vol. 57, no. 10, pp. 2339–2344, 2015.

[24] S. Doddipalli, A. Kothari, and P. Peshwe, "A low profile ultrawide band monopole antenna for wearable applications," *International Journal of Antennas and Propagation*, vol. 2017, Article ID 7362431, 9 pages, 2017.

[25] M. A. Kenari and M. N. Moghadasi, "UWB miniature antenna based on the CRLH-TL with increase gain for electromagnetic requirements," *Advanced Electromagnetics*, vol. 3, no. 1, pp. 61–65, 2014.

[26] M. Alibakhshi-Kenari, M. Movahhedi, and H. Naderian, "A new miniature ultra wide band planar microstrip antenna based on the metamaterial transmission line," in *Proceedings of the IEEE Asia-Pacific Conference on Applied Electromagnetics (APACE)*, pp. 293–297, Melaka, Malaysia, December 2012.

[27] S. Bhattacharjee, S. Maity, S. K. Metya, and C. T. Bhunia, "Performance enhancement of implantable medical antenna using differential feed technique," *Engineering Science and Technology, an International Journal*, vol. 19, no. 1, pp. 642–650, 2016.

[28] U. Ali, S. Ullah, J. Khan et al., "Design and SAR analysis of wearable antenna on various parts of human body, using conventional and artificial ground planes," *Journal of Electrical Engineering and Technology*, vol. 12, no. 1, pp. 317–328, 2017.

[29] B. N. Balarami Reddy, P. Sandeep Kumar, T. Rama Rao, N. Tiwari, and M. Balachary, "Design and analysis of wideband monopole antennas for flexible/wearable wireless device applications," *Progress In Electromagnetics Research M*, vol. 62, pp. 167–174, 2017.

[30] B. Sugumaran, R. Balasubramanian, and S. K. Palaniswamy, "Reduced specific absorption rate compact flexible monopole antenna system for smart wearable wireless communications," *Engineering Science and Technology, an International Journal*, vol. 24, no. 3, pp. 682–693, 2021.

[31] S. Shrestha, M. Agarwal, P. Ghane, and K. Varahramyan, "Flexible microstrip antenna for skin contact application," *International Journal of Antennas and Propagation*, vol. 2012, Article ID 745426, 5 pages, 2012.